

Supporting Information

Towards efficient NFA-based selective near-infrared organic photodetectors: impact of thermal annealing of polymer blends

Q. Eynaud,^a Y. A. Avalos Quiroz,^a T. Koganezawa,^b R. Sato,^c N. Yoshimoto,^c O. Margeat,^a C. M. Ruiz,^d J. Ackermann,^a C. Videlot-Ackermann^{*,a}

^a Aix Marseille Univ., CNRS, CINAM, Marseille, France

^b Industrial Application Division, Japan Synchrotron Radiation Research Institute (JASRI), Sayo, Hyogo 679-5198, Japan.

^c Department of Physical Science and Materials Engineering, Iwate University, Ueda Morioka 020 8551, Japan.

^d Aix Marseille Univ., Univ. de Toulon, UMR CNRS 7334, IM2NP, Marseille, France

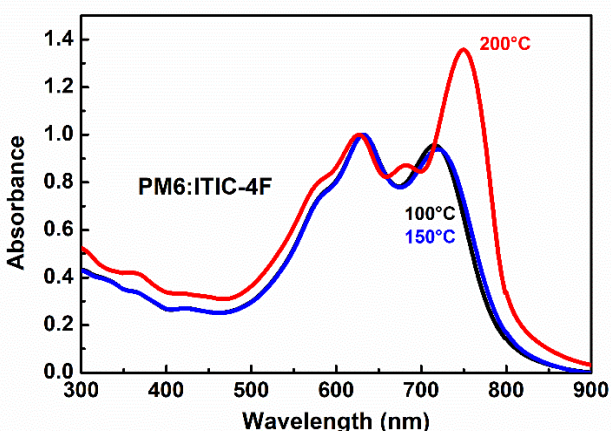


Figure S1. Normalized absorption spectra of PM6:ITIC-4F (1:2 w/w ratio) blend layers as function of thermal annealing temperature.

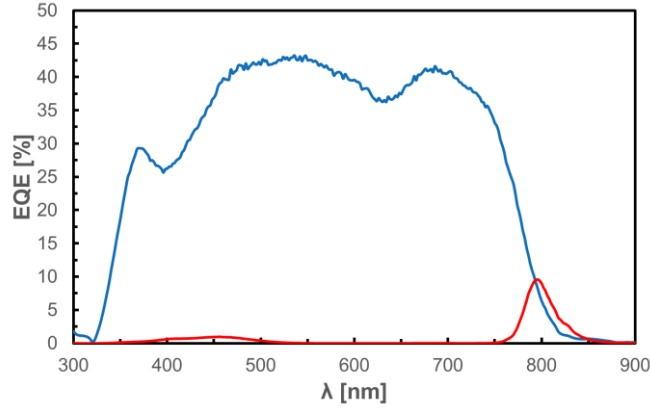


Figure S2. External quantum efficiency (EQE) spectra of photodiode devices in normal structure as ITO/PEDOT:PSS/PM6:ITIC-4F/ZnO/Al. PM6:ITIC-4F blends: 1:1 w/w ratio, annealed at 100°C and 200 nm thick (large band in blue) or > 2 μm thick (narrowband in red). EQE realized under a bias of 0 V.

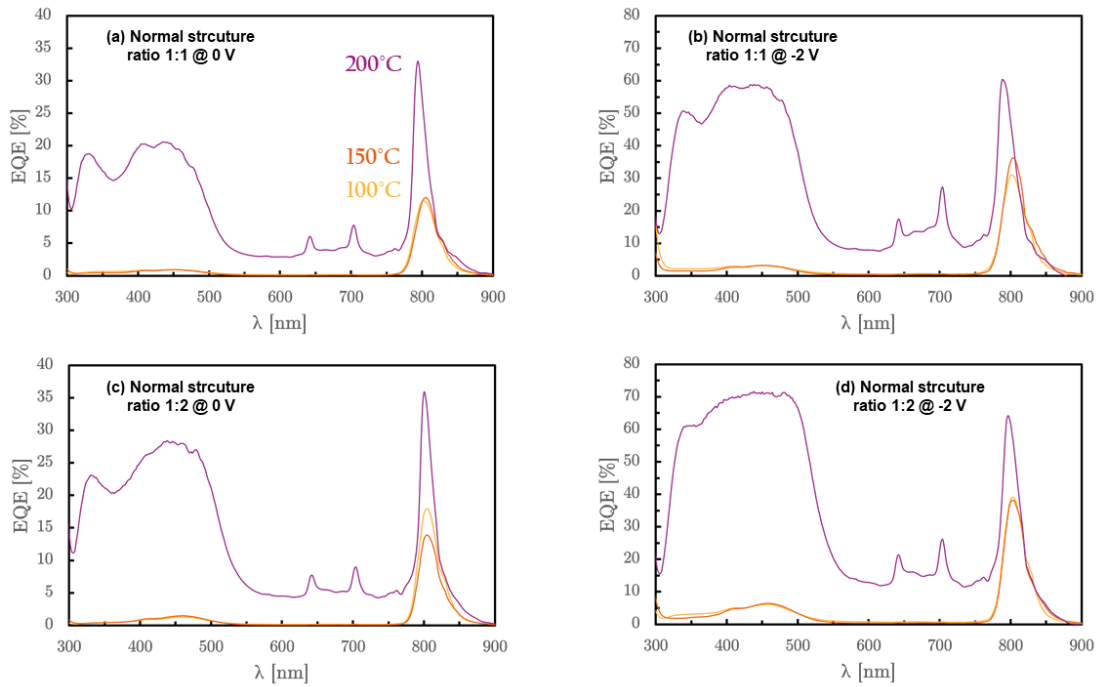


Figure S3. External quantum efficiency (EQE) spectra of OPDs in normal structure as ITO/PEDOT:PSS/PM6:ITIC-4F/ZnO/Al by varying the thermal annealing temperature of the active layers from 100 to 200°C under a bias of 0 V and -2 V. PM6:ITIC-4F blends: 1:1 or 1:2 w/w ratio, > 2 μm thick.

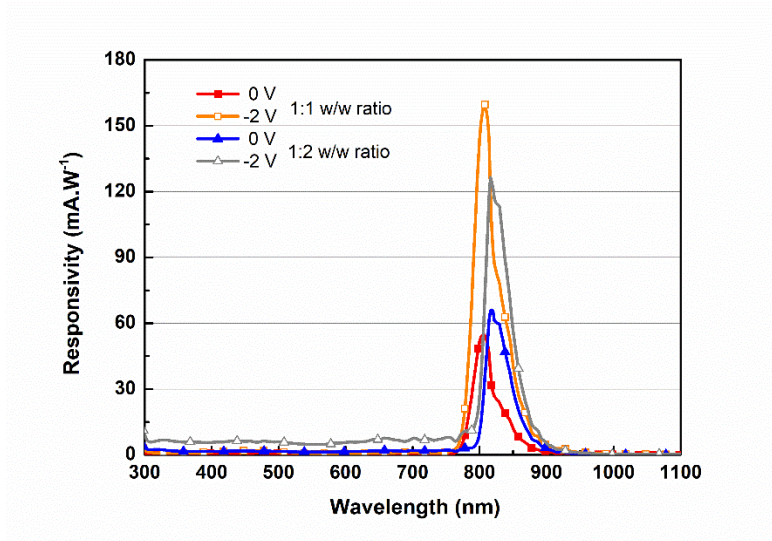


Figure S4. Calculated responsivity spectra of OPDs from the EQE measurement. OPDs in inverted structure as ITO/ZnO/PM6:ITIC-4F/MoO₃/Ag under biases 0 V and -2 V. PM6:ITIC-4F blends: 1:1 or 1:2 w/w ratio, annealed at 200°C, > 2 μm thick.

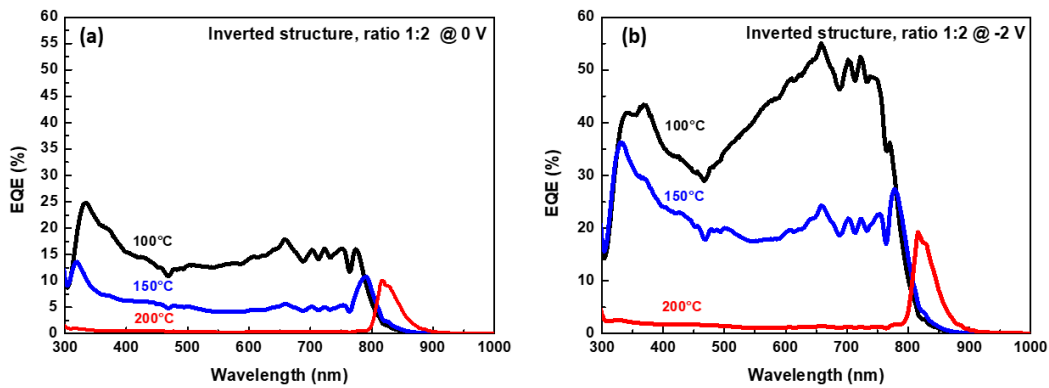


Figure S5. External quantum efficiency (EQE) spectra of OPDs in inverted structure as ITO/ZnO/PM6:ITIC-4F(1:2 w/w ratio, > 2 μm thick)/MoO₃/Ag and by varying the thermal annealing of the active layers from 100 to 200°C under different biases (a) 0 V and -2 V (b).

Table S1. Thickness and OPD parameters of devices in normal and inverted structures at 0 V and -2 V biases for 1:1 and 1:2 w/w ratio.

| | | 1:1 ratio | | | | | | | | | | |
|-------|------------------|-----------|-------------------------|------------------------|--|----------------|--------------------|-------------------------|------------------------|--|----------------|--------------------|
| | | 0 V | | | | | | -2 V | | | | |
| | | d (μm) | λ_{EQEmax} (nm) | EQE ⁽³⁾ (%) | $\mathfrak{R}_{max}^{(4)}$ (mA.W ⁻¹) | FWHM (nm) | SRR ⁽⁵⁾ | λ_{EQEmax} (nm) | EQE ⁽³⁾ (%) | $\mathfrak{R}_{max}^{(4)}$ (mA.W ⁻¹) | FWHM (nm) | SRR ⁽⁵⁾ |
| 100°C | I ⁽¹⁾ | 2.52 | 782 | 11.0 | 69.3 | 30 | 6.6 | 777 | 24.5 | 153.3 | 40 | 3.4 |
| | N ⁽²⁾ | 2.05 | 802 | 11.6 | 74.9 | 38 | 21.3 | 802 | 31.0 | 200.2 | 40 | 17.1 |
| 150°C | I ⁽¹⁾ | 2.52 | 796 | 10.9 | 69.8 | 30 | 31.3 | 800 | 28.8 | 185.5 | 41 | 22.5 |
| | N ⁽²⁾ | 2.37 | 806 | 12.1 | 78.5 | 41 | 23.7 | 804 | 36.3 | 235.5 | 38 | 20.4 |
| 200°C | I ⁽¹⁾ | 2.74 | 806 | 8.45 | 54.8 | 44 | 74.2 | 807 | 24.5 | 159.6 | 42 | 80.5 |
| | N ⁽²⁾ | 2.02 | 794 | 33.0 | 211 | 22 | 2.9 ⁽⁶⁾ | 788 | 60.4 | 383.3 | 35 | 1.8 ⁽⁶⁾ |
| | | 1:2 ratio | | | | | | | | | | |
| | | 0 V | | | | | | -2 V | | | | |
| | | d (μm) | λ_{EQEmax} (nm) | EQE ⁽³⁾ (%) | $\mathfrak{R}_{max}^{(4)}$ (mA.W ⁻¹) | FWHM (nm) | SRR ⁽⁵⁾ | λ_{EQEmax} (nm) | EQE ⁽³⁾ (%) | $\mathfrak{R}_{max}^{(4)}$ (mA.W ⁻¹) | FWHM (nm) | SRR ⁽⁵⁾ |
| 100°C | I ⁽¹⁾ | 2.23 | ₍₆₎ | ₍₆₎ | ₍₆₎ | ₍₆₎ | ₍₆₎ | ₍₆₎ | ₍₆₎ | ₍₆₎ | ₍₆₎ | ₍₆₎ |
| | N ⁽²⁾ | 2.27 | 804 | 17.9 | 115.9 | 38 | 24.9 | 802 | 39.0 | 251.9 | 41 | 11.2 |
| 150°C | I ⁽¹⁾ | 2.36 | ₍₆₎ | ₍₆₎ | ₍₆₎ | ₍₆₎ | ₍₆₎ | ₍₆₎ | ₍₆₎ | ₍₆₎ | ₍₆₎ | ₍₆₎ |
| | N ⁽²⁾ | 2.32 | 804 | 13.9 | 90 | 38 | 16.6 | 804 | 38.2 | 247.3 | 38 | 10.4 |
| 200°C | I ⁽¹⁾ | 2.27 | 818 | 10 | 65.8 | 41 | 38.1 | 816 | 19.2 | 126.2 | 43 | 20.5 |
| | N ⁽²⁾ | 2.37 | 800 | 35.9 | 231 | 22 | 2.2 ⁽⁶⁾ | 796 | 64.2 | 411.6 | 32 | 1.5 ⁽⁶⁾ |

- (1) Inverted structure
- (2) Normal structure
- (3) EQE at λ_{EQEmax}
- (4) Responsivity $\mathfrak{R}_{max} = EQE \times (\lambda q/hc)$ calculated with EQE at λ_{EQEmax}
- (5) SRR: spectral rejection ratio (Responsivity \mathfrak{R} ratio of highest value to that at 460 nm)
- (6) No CCN-type OPDs identified from EQE spectra or from SRR value (<3).

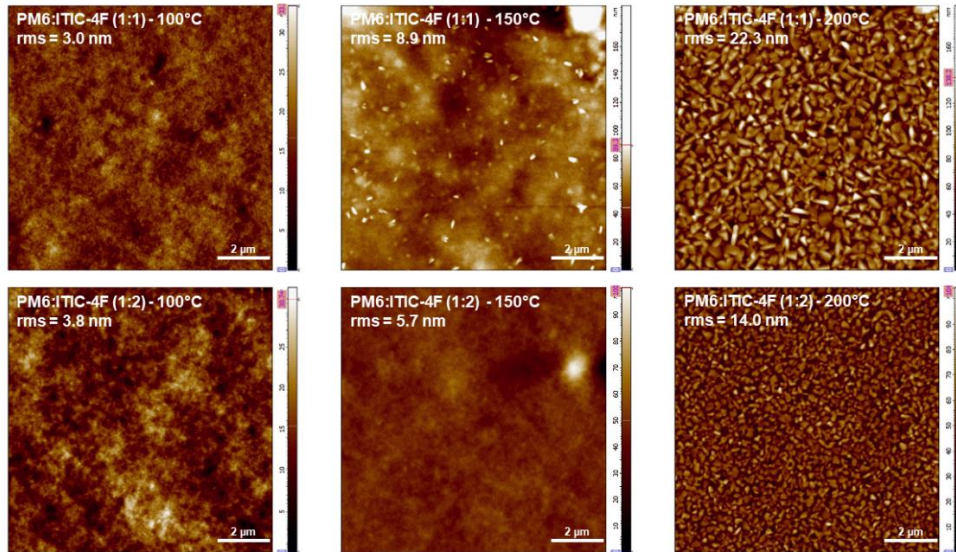


Figure S6. Atomic force microscopy (AFM) height images of PM6:ITIC-4F bulk heterojunction blends (1:1 w/w ratio on top and 1:2 w/w ratio on bottom) annealed at 100°C, 150°C and 200°C. Scale: 10×10 μm².

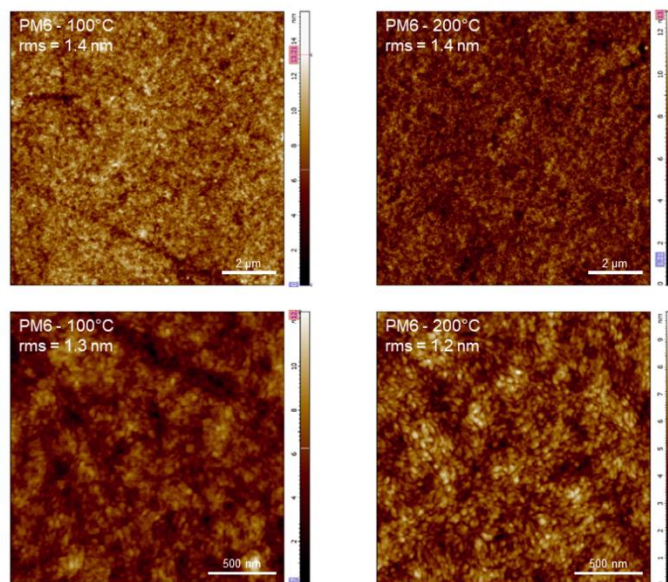


Figure S7. Atomic force microscopy (AFM) height images of neat PM6 layers annealed at 100°C and 200°C. Scales: on top $10 \times 10 \mu\text{m}^2$ and on bottom $2 \times 2 \mu\text{m}^2$.

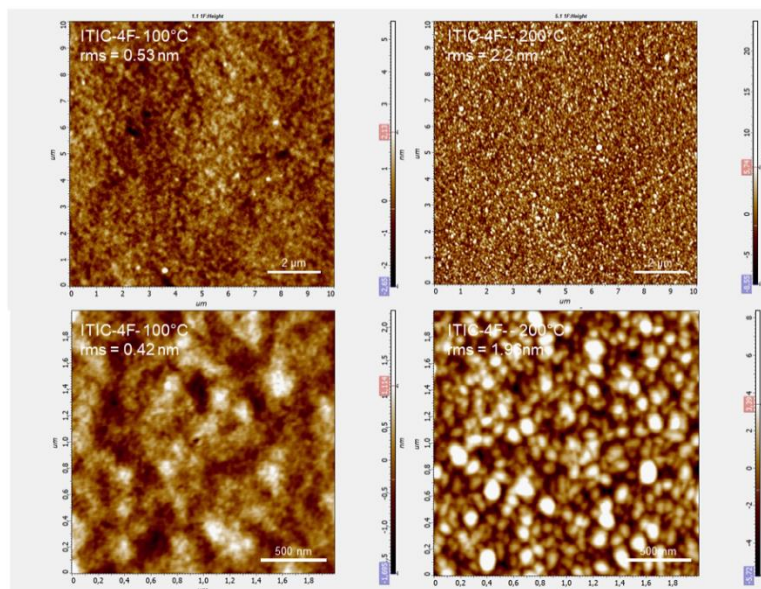


Figure S8. Atomic force microscopy (AFM) height images of neat ITIC-4F layers annealed at 100°C and 200°C. Scales: on top $10 \times 10 \mu\text{m}^2$ and on bottom $2 \times 2 \mu\text{m}^2$.

Table S2. Root mean square (rms) roughness and water contact angle (WCA) data of neat films (PM6 and ITIC-4F) and PM6:ITIC-4F blends in 1:1 and 1:2 w/w ratio.

| Material | Temperature (°C) | rms roughness ⁽¹⁾ (nm) | Average WCA (°) | Min. WCA (°) | Max. WCA (°) | Stan. Dev. (°) |
|-------------------------|------------------|-----------------------------------|-----------------|--------------|--------------|----------------|
| PM6 | 100 | 1.3 | 101 | 100.81 | 101.19 | 0.14 |
| | 200 | 1.2 | 100.5 | 100.38 | 100.76 | 0.18 |
| ITIC-4F | 100 | 0.42 | 93.6 | 91.97 | 94.77 | 1.07 |
| | 200 | 1.96 | 92.7 | 91.09 | 93.85 | 1.09 |
| PM6:ITIC-4F (ratio 1:1) | 100 | 2.1 | 102.7 | 101.64 | 103.81 | 0.79 |
| | 150 | 3.8 | 105.3 | 104.41 | 106.02 | 0.58 |
| | 200 | 21.8 | 108.0 | 107.56 | 108.27 | 0.30 |
| PM6:ITIC-4F (ratio 1:2) | 100 | 2.5 | 101.1 | 100.91 | 101.30 | 0.17 |
| | 150 | 2.3 | 100.5 | 100.40 | 100.67 | 0.12 |
| | 200 | 11.3 | 107.4 | 106.14 | 108.50 | 0.90 |

⁽¹⁾ From AFM pictures with a scale 2x2 μm^2 .

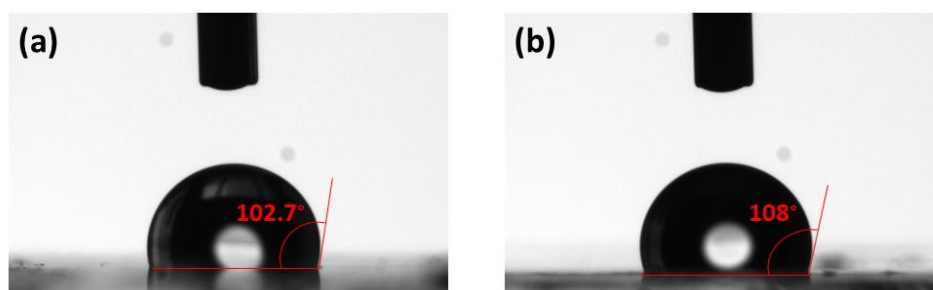


Figure S9. Water contact angle (WCA) images of PM6:ITIC-4F blends in 1:1 w/w ratio at 100°C (a) and 200°C (b)

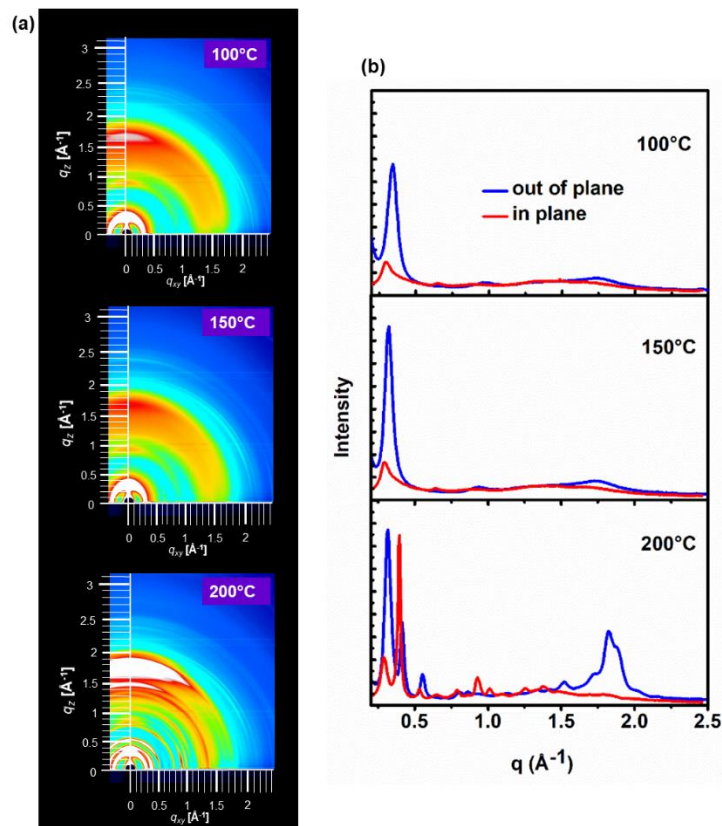


Figure S10. 2D-GIXRD patterns (a) and corresponding in plane and out of plane profiles (b) of PM6:ITIC-4F (1:2 w/w ratio) films deposited on ZnO buffer layer as function of thermal annealing temperature.

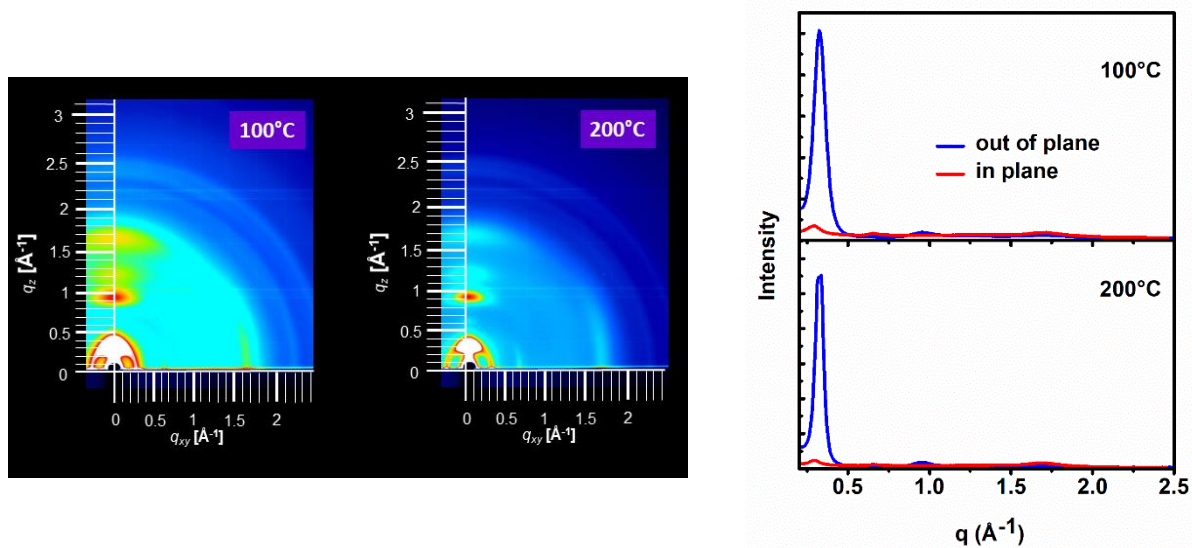


Figure S11. 2D-GIXRD patterns and corresponding profiles (in plane and out of plane) of PM6 thin films deposited on ZnO buffer layer as function of thermal annealing temperature.

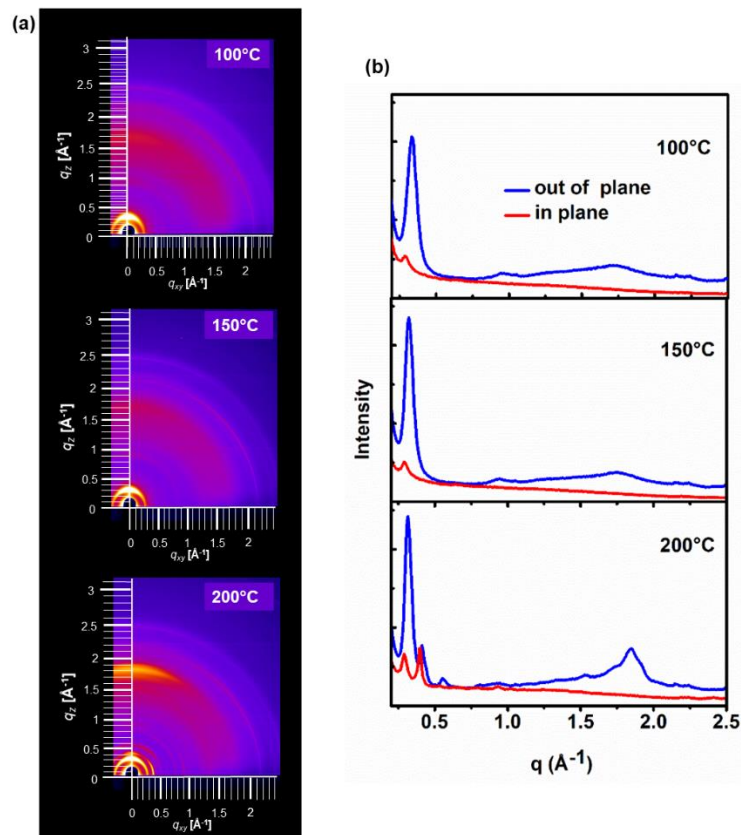


Figure S12. 2D-GIXRD patterns (a) and corresponding in plane and out of plane profiles (b) of PM6:ITIC-4F (1:1 w/w ratio) films deposited on PEDOT:PSS buffer layer as function of thermal annealing temperature.

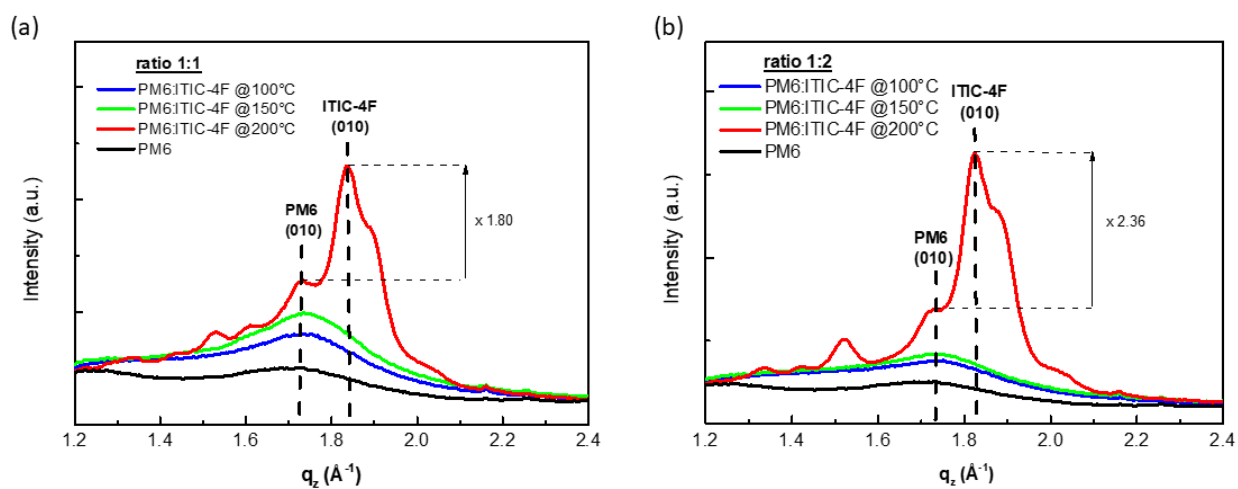


Figure S13. Zoom in OOP profiles of neat PM6 and PM6:ITIC-4F films deposited on ZnO buffer layer as function of thermal annealing temperature in (a) 1:1 and (b) 1:2 w/w ratio.

Table S3. XRD data of PM6:ITIC-4F (1:1 and 1:2 w/w ratio) blend layers deposited on ZnO buffer layer as function of thermal annealing temperature (100°C, 150°C and 200°C). Additionally, data of blend at 200°C deposited on PEDOT:PSS are given for comparison.

| Ratio | T (°C) | | q_z (\AA^{-1}) (100) peak | Peak area ⁽¹⁾ | Peak area in % ⁽²⁾ | FMHW ⁽³⁾ | d ⁽⁴⁾ (nm) | CCL ⁽⁵⁾ (nm) |
|--------------------|---------|---------|--|--------------------------|-------------------------------|---------------------|-------------------------|-------------------------|
| 1:1 | 100 | PM6 | 0.337 | 30571.7 | 98.3 | 0.07987 | 1.86 | 1.12 |
| | | ITIC-4F | 0.421 | 520.6 | 1.7 | 0.04001 | 1.50 | 2.25 |
| | 150 | PM6 | 0.323 | 32935 | 90.8 | 0.06214 | 1.94 | 1.45 |
| | | ITIC-4F | 0.403 | 3328 | 9.2 | 0.05204 | 1.55 | 1.73 |
| | 200 | PM6 | 0.318 | 23981.4 | 80.7 | 0.05399 | 1.97 | 1.66 |
| | | ITIC-4F | 0.405 | 5731.3 | 19.3 | 0.04169 | 1.54 | 2.16 |
| 200 ⁽⁶⁾ | PM6 | 0.318 | 4979.9 | 87.7 | 0.05087 | 1.97 | 1.77 | |
| | ITIC-4F | 0.414 | 693.7 | 12.3 | 0.04082 | 1.51 | 2.2 | |
| 1:2 | 100 | PM6 | 0.341 | 16374.8 | 98.3 | 0.07052 | 1.84 | 1.27 |
| | | ITIC-4F | 0.409 | 270.8 | 1.7 | 0.03398 | 1.53 | 2.65 |
| | 150 | PM6 | 0.322 | 19019.1 | 94 | 0.05677 | 1.94 | 1.58 |
| | | ITIC-4F | 0.408 | 1206.4 | 6 | 0.04234 | 1.54 | 2.12 |
| | 200 | PM6 | 0.317 | 17650.1 | 78.1 | 0.05021 | 1.97 | 1.80 |
| | | ITIC-4F | 0.414 | 4938.2 | 21.9 | 0.03393 | 1.51 | 2.65 |
| PM6 | 100 | | 0.327 | | | 0.08185 | 1.92 | 1.10 |
| | 200 | | 0.325 | | | 0.05666 | 1.93 | 1.58 |

- (1) peak area after deconvolution
- (2) contribution to the area of the cumulative fit peak
- (3) FMHW = full width at half maximum
- (4) $d = 2 \pi/q$
- (5) CCL for crystal coherence length
- (6) Blend on PEDOT:PSS

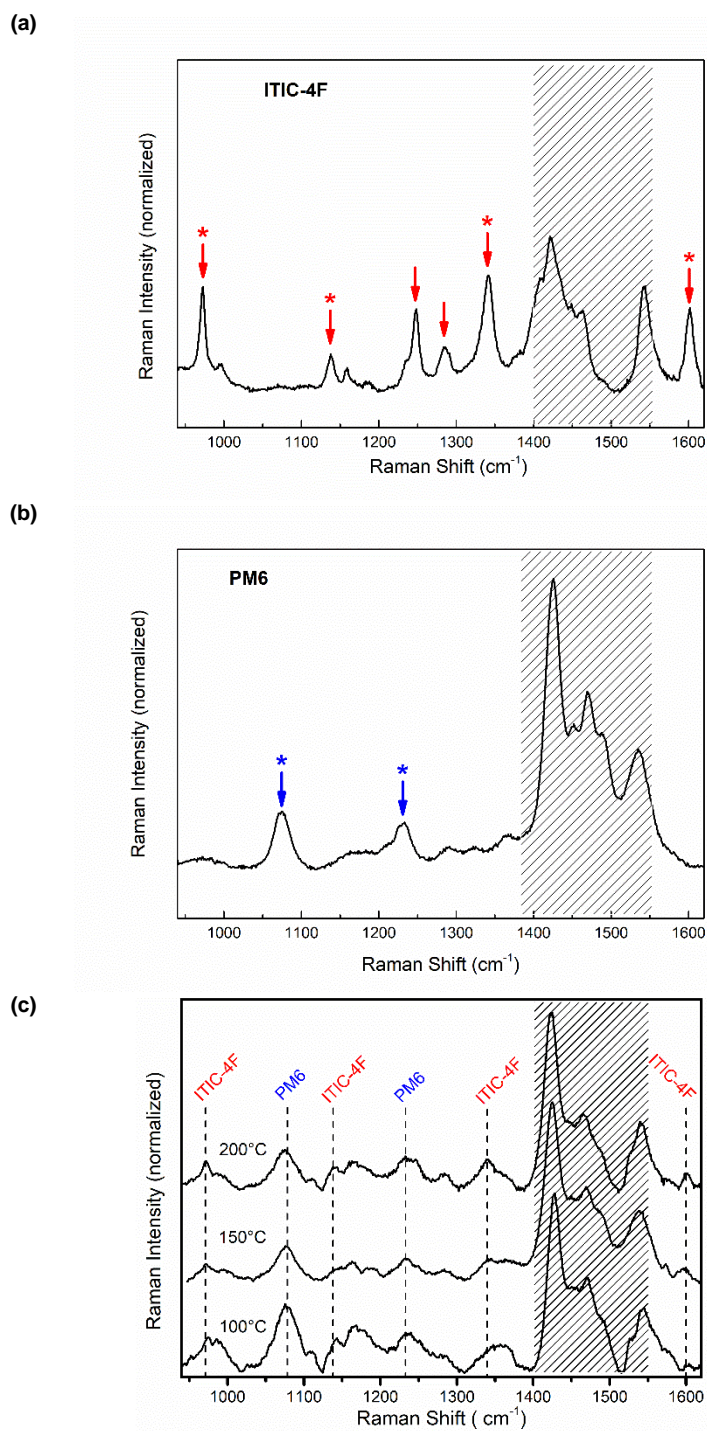


Figure S14. Raman spectra of neat ITIC-4F (a) and PM6 (b) layers annealed at 200°C. (c) Raman spectra from the back side of PM6:ITIC-4F blends with 1:1 w/w ratio annealed at 100°C, 150°C and 200°C. Thickness: ~ 100 nm for (a) and (b), > 2 μm for (c).

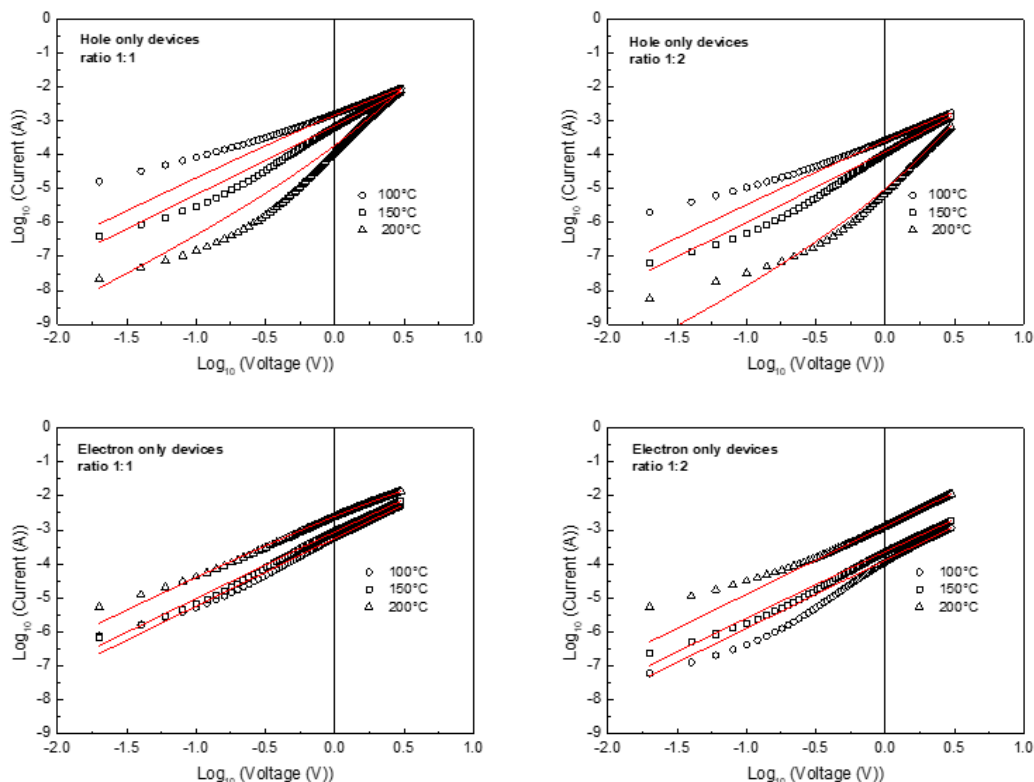


Figure S15. Current vs. voltage for holes and electron only devices based on PM6:ITIC-4F blends with 1:1 and 1:2 w/w ratio. The charges carrier mobility values of PM6:ITIC-4F blends were determined following the single-carrier devices SCLC model.

Table S4. Thickness (d), hole (μ_h) and electron (μ_e) mobility values obtained by SCLC of PM6:ITIC-4F bulk heterojunction layers as function of blend ratio, thermal annealing temperature and thickness. Standard deviations are indicated in brackets, from measurements on 6 devices.

| ratio | Thermal annealing temperature | Hole only devices | | Electron only devices | | μ_e/μ_h |
|-------|-------------------------------|--------------------|--|-----------------------|---|-------------------|
| | | thickness d (nm) | μ_h (cm ² /V.s) | thickness d (nm) | μ_e (cm ² /V.s) | |
| 1:1 | 100°C | 149 (\pm 2.5) | 2.46×10^{-4} (\pm 1.9×10^{-5}) | 129 (\pm 22) | 3.27×10^{-5} (\pm 4.05×10^{-6}) | 0.13 |
| | 150°C | 146 (\pm 4.5) | 6.31×10^{-5} (\pm 6.4×10^{-6}) | 140 (\pm 9) | 7.9×10^{-5} (\pm 7.65×10^{-6}) | 1.25 |
| | 200°C | 146 (\pm 10) | 1.79×10^{-6} (\pm 3.6×10^{-7}) | 136 (\pm 6.5) | 3.68×10^{-4} (\pm 1.8×10^{-5}) | 205 |
| | 100°C | 1257 (\pm 15) | 1.66×10^{-5} (\pm 0.5×10^{-5}) | 1818 (\pm 40) | nd ⁽¹⁾ | nd ⁽¹⁾ |
| | 200°C | 1270 (\pm 35) | 4.05×10^{-6} (\pm 4.2×10^{-6}) | 1821 (\pm 70) | 5.9×10^{-4} (\pm 1.5×10^{-5}) | 145 |
| 1:2 | 100°C | 236 (\pm 15.5) | 1.32×10^{-4} (\pm 5.5×10^{-6}) | 271 (\pm 10) | 8.21×10^{-5} (\pm 6.7×10^{-6}) | 39 |
| | 150°C | 243 (\pm 12) | 3.71×10^{-5} (\pm 2.4×10^{-6}) | 276 (\pm 12.5) | 1.72×10^{-4} (\pm 1.65×10^{-5}) | 4.6 |
| | 200°C | 228 (\pm 13.5) | 1.98×10^{-7} (\pm 5.1×10^{-8}) | 266 (\pm 12) | 6.71×10^{-4} (\pm 9×10^{-6}) | 3388 |

(1) Not determined: SCLC protocol could not be applied to the curves resulting from the measurement. To apply SCLC protocol, I-V data should include two or three complete sweep cycles from zero volt to positive voltage, then to negative voltage and finally to the point of origin. These sweeps should be free of hysteresis.[1]

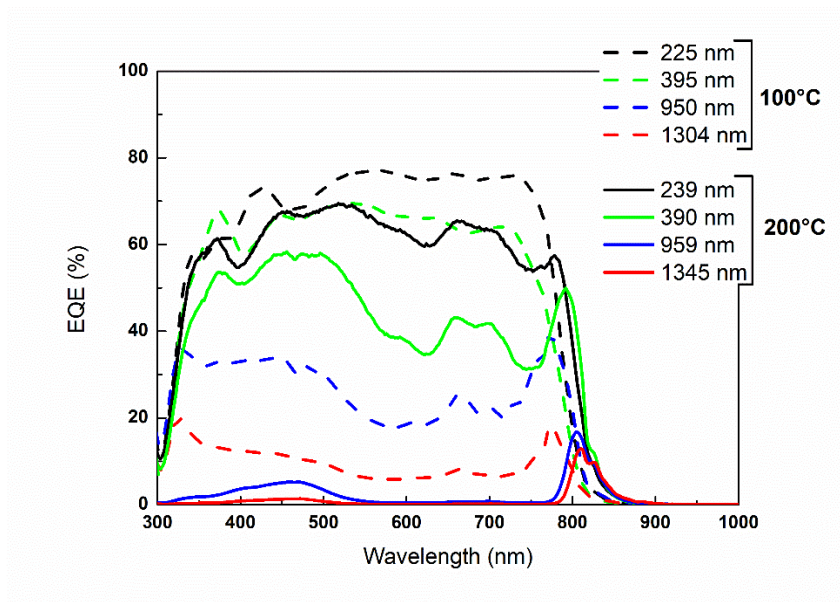


Figure S16. External quantum efficiency (EQE) spectra of OPDs in inverted structure ITO/ZnO/PM6:ITIC-4F(1:1 w/w ratio)/MoO₃/Ag as function of PM6:ITIC-4F thickness and post-annealing temperature.

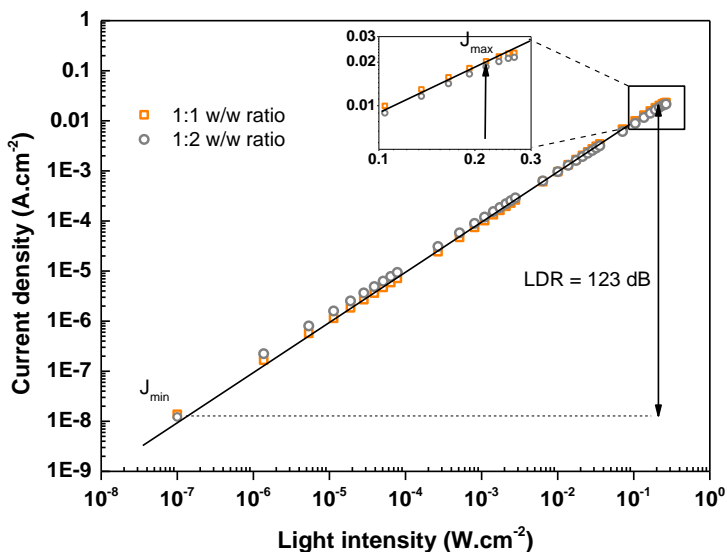


Figure S17. Linear dynamic range (LDR) for the OPD measured at -2 V (pump wavelength ~810 nm).

[1] S. Ben Dkhil, P. Perkhun, C. Luo, D. Müller, R. Alkarsifi, E. Barulina, Y. A. Avalos Quiroz, O. Margeat, S. T. Dubas, T. Koganezawa, D. Kuzuhara, N. Yoshimoto, C. Caddeo, A. Mattoni, B. Zimmermann, U. Würfel, M. Pfanmöller, S. Bals, J. Ackermann and C. Vidolot-Ackermann, *ACS Appl. Mater. Interfaces*, 2020, **12**, 28404.